

Mitigation of expansive deterioration processes through crack control

C.P. Ostertag, J. Blunt & J. Grubb
University of California, Berkeley, CA, USA

ABSTRACT: Damage due to corrosion and alkali silica reaction is being mitigated through crack control. The paper discusses how durability can be enhanced by controlling microcracking in close vicinity to the reaction sites, which limits the egress of reaction products away from the reaction site. Mortar specimens with and without microfibers were exposed to either alkaline or corrosive environments. Crack control on the microscale in close vicinity to the reaction site reduced both the alkali silica reaction rate and the corrosion rate. Corrosion current density measurements based on polarization resistance and Tafel measurements indicate that the microfiber-reinforced specimens are more resistant to corrosion than the unreinforced control specimens.

1 INTRODUCTION

The concrete infrastructure in the US and in most industrialized countries is deteriorating at a faster pace than predicted. According to the Civil Engineering Research Foundation, the US has an estimated \$1 trillion in deteriorated concrete structures including bridges, highways, piers, wharfs, structures and buildings (Cerf 2004).

There are four main deterioration mechanisms in concrete: Corrosion, Frost Action, Alkali Silica Reaction (ASR) and Sulfate attack (Rostam 2001). The common approach to enhance durability addresses each of the deterioration processes in isolation and recommends different remedies for each deterioration mechanism because each process (i.e. corrosion, frost action, ASR, sulfate attack) involves different reactants. However, all these deterioration processes have one common signature: they are expansive and cause cracking. Cracks allow the ingress of water and aggressive agents into the interior of concrete, thereby accelerating the deterioration process. Hence crack control is paramount in order to mitigate damage in concrete structures. Furthermore, cracks initiate as small microcracks. Therefore, to minimize damage the initiation and propagation of microcracks needs to be controlled and their coalescence into macrocracks significantly delayed.

The effect of crack control from the micro to the macrolevel on mechanical properties is briefly discussed. However, the emphasis of this paper is on the effect of crack control on expansive deterioration processes such as alkali silica reaction (ASR) and corrosion. ASR is a chemical reaction between alkalis from cement and certain forms of silica present in aggregates. The chemical reaction forms an ASR gel that imbibes water resulting in volumetric expansion. This volumetric expansion causes cracking in cement based materials if the expansion pressure exceeds the tensile capacity of the matrix. Corrosion is also an expansive process. When reinforcing steel within concrete corrodes, the rust product applies expansive pressure on the surrounding concrete inducing cracking in the matrix in close vicinity to the reinforcing steel. Since cracks initiate as microcracks in close vicinity to the reaction site, this paper focuses on the effect of crack control on the microscale on alkali silica reaction rate and corrosion rate.

2 MECHANICAL PERFORMANCE ENHANCEMENT DUE TO CRACK CONTROL

Crack control from the micro to the macrolevel enhances the mechanical properties of reinforced concrete as shown in Figure 1. In this case crack

control was achieved through fiber hybridization. The hybrid fiber reinforced concrete (HyFRC) composite shown in Figure 1 was developed for the use in bridge approach slabs exposed to severe environmental conditions (Blunt & Ostertag 2007). The composite utilizes two types of fibers, macrofibers (conventional fibers) and microfibers. The microfibers control the microcracks and the macrofibers control and resist propagation of macrocracks. Figure 1 shows that fiber hybridization provides deflection hardening which delays macrocrack formation until more than twice the load levels when compared to control specimens (plain concrete). The HyFRC and control specimens both contain coarse aggregates and conventional steel reinforcements and were tested in four point bending. The concept of micro and macrofiber hybridization has been used by other researchers (Quian & Stroeven 2000; Banthia & Soleimani 2005) to primarily enhance the mechanical performance of cement based composites. HyFRC composites have not yet been applied to study the effect of crack control on expansive deterioration processes.

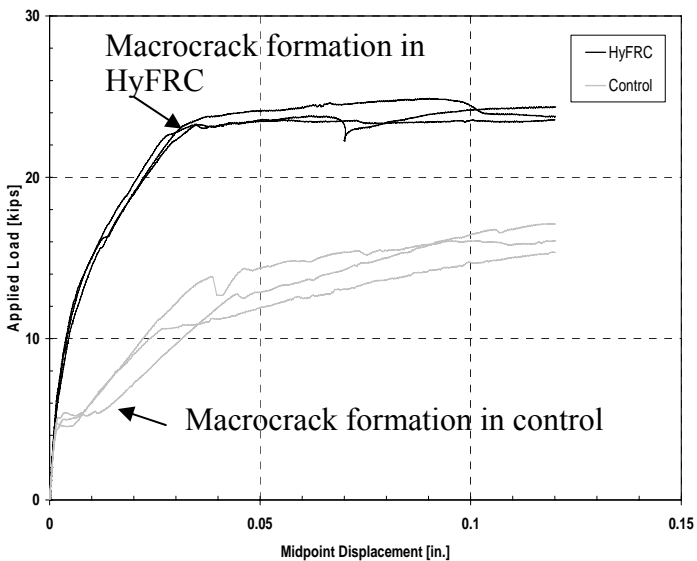


Figure 1. Enhancement in mechanical properties due to crack control

Cracks due to expansive deterioration processes initiate as microcracks in close vicinity to the reaction site. The microfibers in HyFRC composites due to their small diameter are able to bridge these microcracks at onset as shown in Figure 2 contrary to macrofibers which are not only too thick but also spaced too far apart to influence these microcracks. Furthermore, microfibers exhibit steep crack growth resistance behavior due to toughening mechanisms associated with crack fiber interactions (Yi & Ostertag 2002, 2007). The focus of this paper is on

the effect of crack control on the microscale on expansive deterioration processes such as alkali silica reaction and corrosion.

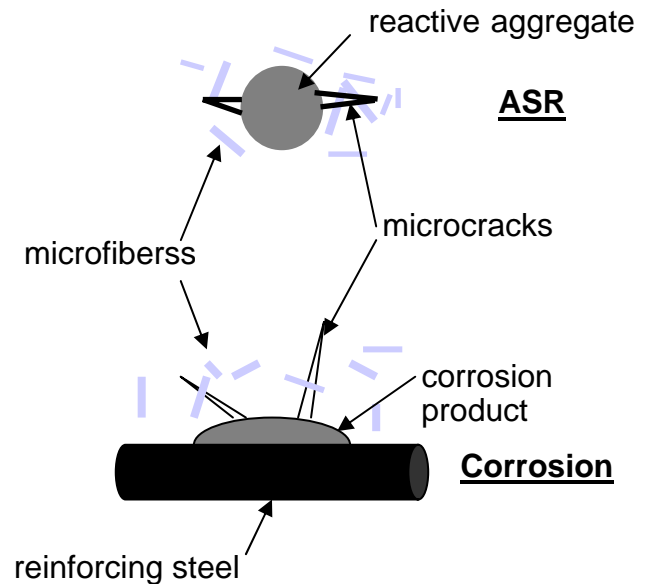


Figure 2. Microcracks caused by either ASR or corrosion are being controlled by microfibers in close vicinity to the reaction sites.

The difference in crack growth behavior between unreinforced (control) and microfiber reinforced specimens is illustrated schematically in Figure 3. Let's assume a crack initiates at time t_1 at the reaction site (i.e. either reactive aggregate/matrix interface or steel reinforcing bar/matrix interface) in the control specimen. The small resistance to crack extension in the control specimen is shown by the large increase in crack length and crack opening displacement with increasing exposure time to either NaOH or NaCl solution at t_2 and t_3 . The lack of crack growth resistance behavior in the unreinforced specimens reduces the driving force for crack extension, and hence smaller tensile stresses are sufficient to increase the crack length and the accompanying crack width. The crack in the microfiber reinforced specimen (Fig. 3b) initiates at a higher expansion stress (i.e. at exposure time t_2 and not t_1) and extends far less with increasing exposure time due to crack fiber interactions such as crack pinning and crack wake bridging processes (Yi & Ostertag 2007). These energy absorbing mechanisms increase with increasing crack length due to the formation of a bridging zone behind the crack tip. Consequently, not only is a higher expansive pressure (due to ASR or corrosion) required for

cracks to initiate and propagate in microfiber reinforced specimens (Fig. 3b) but the ASR gel is mechanically confined (Yi & Ostertag 2005). Furthermore, microcrack control in close vicinity to the reaction site limits the egress of reaction products away from the reaction site. The effect of delay in crack formation and propagation on ASR and corrosion processes and the effect of preventing the reaction products from leaving the reaction site will be discussed in the following sections.

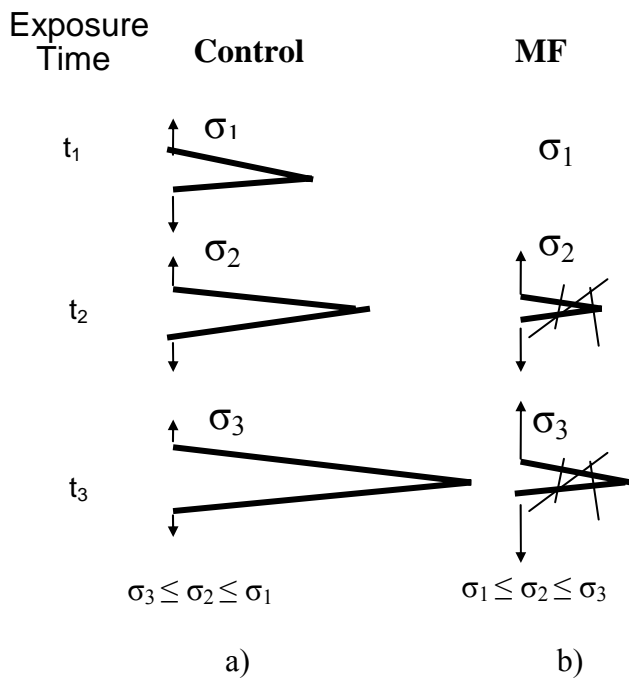


Figure 3. Difference in crack growth behavior of a) control and b) microfiber (MF) reinforced specimens with increasing exposure time, t , to either NaOH (to cause ASR) or NaCl (to cause corrosion).

3 EFFECT OF CRACK CONTROL ON ALKALI SILICA REACTION RATE

The effect of crack control on alkali silica reaction rate was studied in close vicinity to the reactive aggregate using plain and steel microfiber reinforced (SMF) mortar specimens. Rod shaped reactive aggregates of constant diameter were used to investigate differences in ASR gel formation between the SMF reinforced specimens and the control specimens. Each specimen contains a Pyrex rod of 5 mm in diameter as reactive aggregate embedded in its center. Prisms of 2.5x2.5x28.12cm were cast, cured in 80°C water bath for 1 day and immersed in a 1 N NaOH solution stored at 80°C

following the ASTM C-1260 procedure (ASTM 1999). The mortar matrix is reinforced with 0 and 7vol% of steel microfibers (SMF), respectively.

ASR gel formation in SMF reinforced specimens was not only delayed but also the Pyrex rod reacted far less compared to the Pyrex rod embedded in the unreinforced mortar matrices at same exposure times to the NaOH solution. Figure 4a and 4b are backscattered images of the remaining cross-sections of the Pyrex rods for plain and SMF reinforced specimens, respectively, exposed to NaOH solution for 42 days. The reaction starts at the outer surface of the rod and continues towards the center of the Pyrex rod. The dark regions seen between the remaining Pyrex rod and the matrix in Figure 4a and 4b, respectively, will be referred to as the alkali silica reaction rims. In Figure 4a and b, these regions are filled with epoxy used for polishing the specimen surfaces and hence show up dark in the backscattered images. However, these reaction rims are originally filled with solid ASR products and a liquid alkali-silicate solution. Some of the solid ASR products remain but the liquid ASR gel is lost once the samples are sliced off for the sample preparation.

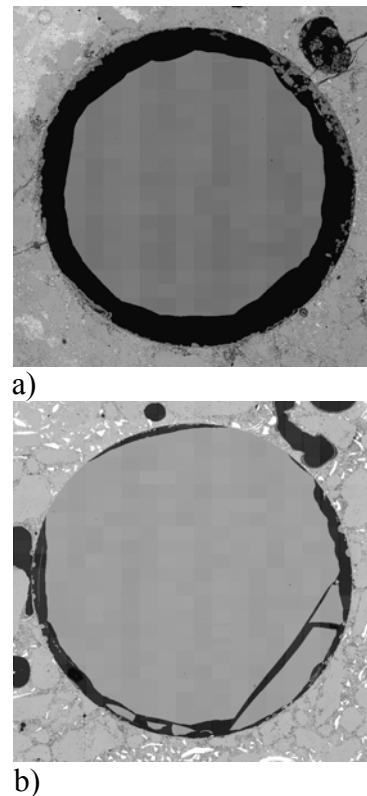


Figure 4. Backscattered (SEM) images of the remaining cross-section of the glass rod after exposure to 1 N NaOH (aq) for 42 days (actual area size: 6mm x 6mm; diameter of glass rod: 5 mm); a) specimen without microfibers, b) specimen reinforced with steel microfibers (visible as white regions in mortar matrix)

The steel microfibers (show up white in the backscattered image) are evenly distributed and in

close proximity to the reactive Pyrex rod. The size of the ASR rim is a function of the dissolution of the rod, the expansion of the matrix due to the gel leaving the reaction sites and swelling in cracks and voids, and the shrinkage of the ASR gel after being exposed to lower relative humidity. Therefore, only the reacted area of the Pyrex rod normalized by its initial area is plotted in Figure 5 as a function of exposure time to NaOH solution. Not only do we observe a delay in ASR gel formation but also a reduction in reactivity of the Pyrex rod in the SMF reinforced specimen compared to the control specimens.

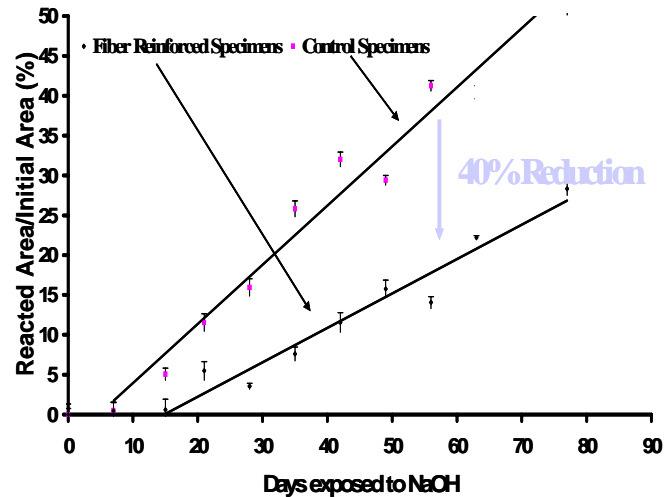


Figure 5. Reacted area of pyrex rod normalized by initial area versus time exposed to 1 N NaOH solution for control and steel microfiber reinforced specimens. The SMF reinforced specimens exhibit a 40% reduction in reaction rate compared to the control specimen (Yi & Ostertag 2005).

The difference in ASR gel formation and ASR rate may be related to the difference in crack formation and crack width between the control and SMF reinforced specimens. Radial cracks that formed due to ASR are visible in Figure 4a but are difficult to see in Figure 4b at the same magnification due to their small crack opening displacements. Table 1 presents results on the ASR rim thickness and the sum of crack widths of the radial cracks measured around the periphery of the reactive aggregate as a function of exposure time to NaOH solution for the control and SMF specimens, respectively. For the unreinforced matrix (Table 1a), both the ASR rim thickness and the crack widths increase with increasing exposure time to NaOH solution. On the other hand, in SMF reinforced specimens no ASR gel formation was observed up to 13 days due to the delay in crack initiation. Once cracks initiated in the SMF reinforced specimens, the width of these cracks were too small to be measured accurately around the Pyrex rod up to exposure time of 27 days in NaOH solution. The

ASR gel formation was considerably reduced in SMF reinforced specimens compared to the control specimens due to the delay in crack initiation and reduced crack width.

Table 1: Average ASR rim thickness and sum of crack width of radial cracks measured around the periphery of the reactive aggregate as a function of exposure time to 1 N NaOH solution for a) unreinforced matrix and b) steel microfiber reinforced matrix

Days	Crack width (Sum), μm	Avg. Rim Thickness, μm	Stand. Dev., Rim, μm
6	41.9	56.5	39.3
13	103.9	41.9	36.2
20	198.5	142.1	96.0
27	176.3	156.9	84.9
37	287.1	178.5	35.0
41	195.2	249.3	139.9

a)

Days	Crack width (Sum), μm	Avg. Rim Thickness, μm	Stand. Dev., Rim, μm
6	0	0	
13	0	0	
20	NA	51.4	18.4
27	NA	16.2	30.5
37	39.2	46.6	9.7
41	52.5	74.7	27.9

b)

The lack of crack control in the control specimens increases the amount of gel formation as shown schematically in Figure 6. Gel formation increases with increasing exposure time to NaOH solution once a crack initiates (at t_2) and increases in width and length (t_3 - t_4). The gel, now able to leave the reaction site fills the cracks and continues to swell, thereby increasing the width and length of the existing cracks which causes the specimen to expand with increasing exposure time to NaOH solution. Gel formation in the SMF reinforced specimens is delayed up to t_3 due to the delay in crack initiation (see also Table 1b). Furthermore, the small crack widths limit the migration of the ASR gel away from the reaction site into the surrounding matrix (t_4). Since the ASR gel can not leave the reaction site, the ion concentration of the ASR products has to be different in the SMF specimens compared to the control specimens. Indeed, this was the case. A higher Na and Si ion concentration was found in the ASR product extracted from the SMF specimens and analyzed by inductive coupled plasma spectroscopy. Because of the higher Si concentration the dissolution of the reactive aggregate in the SMF reinforced specimens is retarded which reduces the reactivity of the reactive aggregate and hence the gel

formation. Viscosity measurements of the liquid ASR products extracted from the SMF and control specimens were conducted using a Rheometrics RMS 800 Rheometer. The liquid ASR gel extracted from the SMF specimens exhibits a 10 fold increase in viscosity compared to the control specimens which further enforces the lack of escape of the reaction products away from the reaction site. The viscosity of alkali silica reaction gels is observed to depend on the Na/Si ratios (Helmuth & Stark 1989).

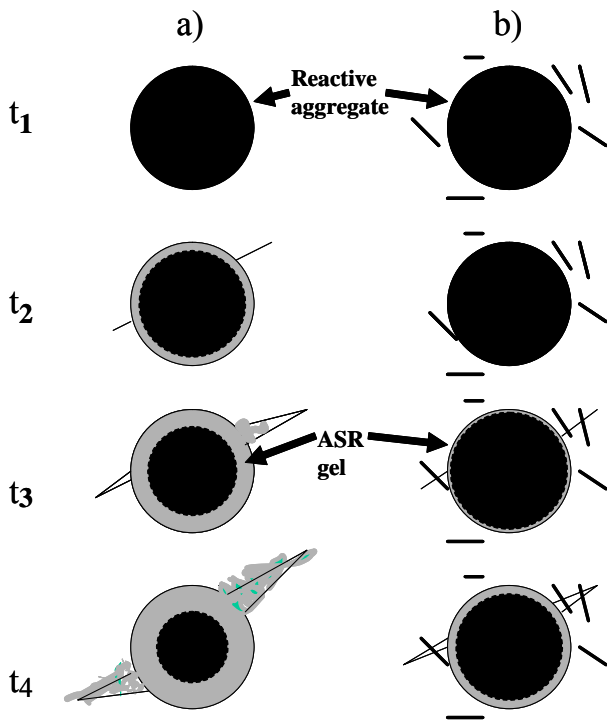


Figure 6. ASR gel formation and reduction in reactive aggregate size with increasing exposure time, t , to NaOH solution; With increasing exposure time the reactive aggregate reacts and decreases in size (dark regions) and the ASR rim thickness increases (i.e. light region between original size of aggregate and remaining aggregate). a) control specimen: ASR gel formation increases and size of original reactive aggregate decreases with increasing exposure time t due to crack formation and increasing crack width. b) SMF reinforced specimen: ASR gel formation and reduction in size of reactive aggregate occur at lower rate due to reduced crack length and reduced crack width associated with crack fiber interactions.

In our case the ASR gel extracted from the reaction sites had the same ratio ($\text{Na/Si}=1$) for both the control and SMF specimens, however, they differ in their ion concentration. Both the Na and Si ion concentration in the SMF reinforced specimens is 33% and 45% higher compared to the control specimen. It was observed in sodium silicate solutions for constant Na/Si ratios of >0.25 that the viscosity increased greatly with the increase in Na concentration (Vail 1952). In our experiment, we

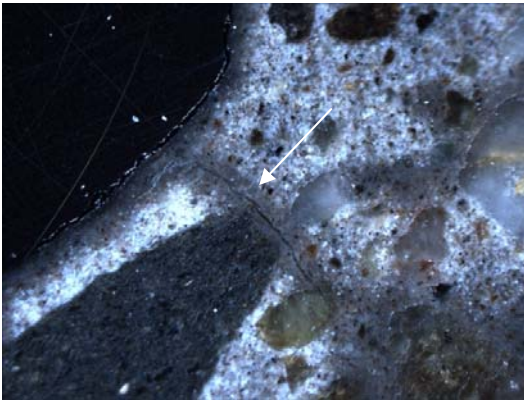
observed an increase in viscosity by a factor of 10 due to an increase in Na concentrations from 3.46 to 4.59 mol/l.

4 EFFECT OF CRACK CONTROL ON CORROSION

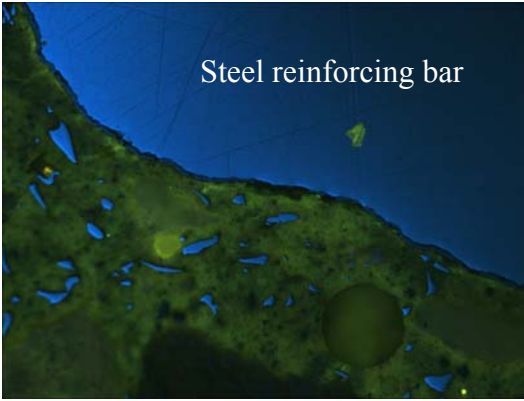
In this study, mortar specimens with and without steel microfiber reinforcements are exposed to a corrosive environment. Microfiber reinforced specimens (4.5% by volume) and control specimens were prepared with water/cement ratios of 0.55 cured for 28 days, and then submerged in aerated 3.5% NaCl solution.

Electrochemical measurements were performed prior to the immersion of the specimens, at 4 weeks of exposure, and at approximately 2-week intervals thereafter up to 7 months. Potentiodynamic polarization measurements were performed with a potentiostat and a three electrode setup. The three electrodes are the working electrode (in this case the steel rebar), the reference electrode and a counter electrode. A stainless steel wire mesh was used as a counter electrode. The specimen preparation and the electrochemical testing procedure is described in detail by Grupp (Grupp et al. 2007). The primary purpose of potentiodynamic tests was to determine the corrosion current (I_{corr}). This is a measure of the rate of charge transfer between the anodic and cathodic reactions at the corrosion potential. The corrosion current density (i_{corr}), denoted by a lower case 'i', is the I_{corr} normalized over the exposed area of steel in the working electrode. The corrosion current density cannot be directly measured, however the anodic/cathodic current differential can. Unfortunately this value is zero at the corrosion potential. Thus various analysis methods were utilized to estimate i_{corr} . These methods included Polarization Resistance, Tafel, and Cyclic Polarization. The same corrosion monitoring cell was used for all tests. The difference was the range to which the specimen was polarized and how the data from the test was analyzed.

Microscopic analysis was performed on the specimens after exposure to NaCl solution for 22 weeks. Radial cracks were observed in the control specimens emanating from the rebar into the mortar as shown in Figure 7a taken under blue fluorescent light. Small spots of corrosion were seen as small red colored areas on the rebar-mortar interface under regular light. No cracks were observed in the SMF reinforced specimens as shown in Figure 7b. Figure 7b provides evidence that the microfibers were located in close vicinity to the steel rebar.



a)



b)

Figure 7. Optical micrographs of a) control and b) microfiber reinforced specimens taken at 5x magnification; radial microcrack in matrix of control specimen is filled with corrosion product; b) no microcracks are observed in the microfiber reinforced specimen. The steel microfibers are in close vicinity to the conventional steel reinforcing bar.

Crack control due to SMF leads to a reduction in corrosion current density (i_{corr}) and hence corrosion rate as shown in Figure 8. The corrosion density is calculated using equation 1 (Gamry 2003).

$$i_{corr} = \frac{B}{r_p} \quad (1)$$

where:

i_{corr} = corrosion current density (units of Current / Area)
 r_p = polarization resistance of the steel ($r_p = \Delta E / \Delta i$ at $E = E_{oc}$)
 B = the Stern-Geary Constant

$$B = \frac{\beta_a \cdot \beta_c}{2.303(\beta_a + \beta_c)} \quad (2)$$

where B is the Stern Geary constant

B is calculated from the anodic (β_a) and cathodic (β_c) Tafel slopes which were determined by the non-linear regression across the experimental Tafel data. R_p is the polarization resistance and the polarization

resistance values are obtained from the tangent of the net current differential between the anodic and cathodic reaction, $I(E)$ curve, at the corrosion potential, E_{oc} . As can be seen from Figure 8, the control specimen exhibits a higher corrosion rate compared to the SMF specimens for the duration of the observation period. The difference in corrosion rates is distinct enough to assert that microfibers reduce the corrosion rate of conventional steel reinforcing bars.

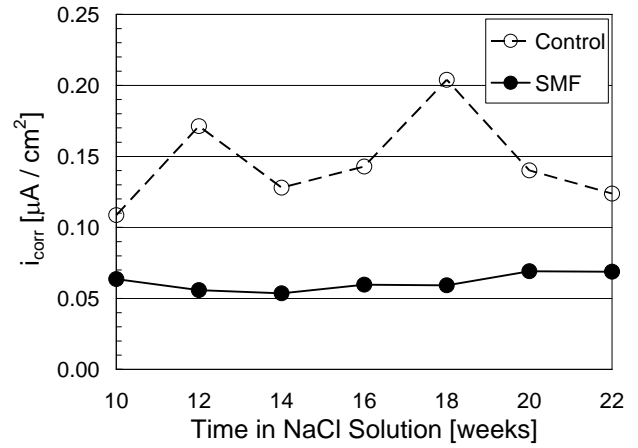


Figure 8. Average Corrosion Current Densities; C stands for control, F for the microfiber specimen.

Cyclic polarization measurements were only made at 22 weeks with a forward scan range of -1.0V to +1.0V. Results on the cyclic polarization measurements, are shown in Figure 9. Observation of the average equilibrium potentials showed that the general tendency was for stabilization within the approximate range of -400mV to -600mV. During this period of stabilization, the least negative value

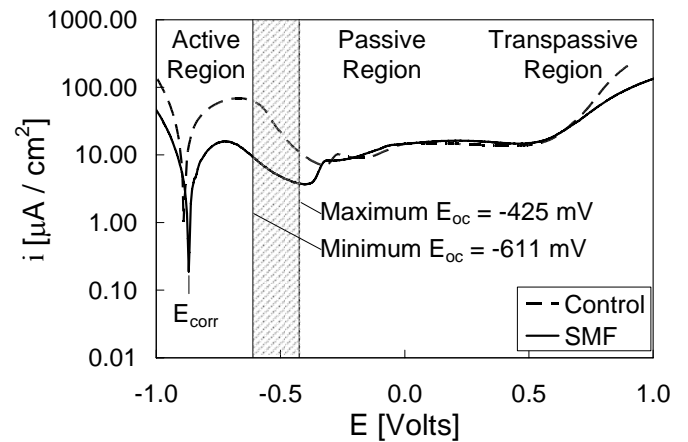


Figure 9. Observed Equilibrium Potential Range Superimposed over 22 Week Forward Polarization Scans; C stands for control specimen, F for steel microfiber specimen.

was -425mV while the most negative value was -611mV. Thus, the corrosion state of the specimens

existed at the border between the active and passive regions (Fig. 9). The region of the polarization curves that is indicative of the actual behavior with respect to corrosion is the region of the equilibrium potentials. Within this region the control specimens had notably higher current densities, signifying the control specimens are more susceptible to corrosion than the microfiber-reinforced specimens.

5 CONCLUSION

Crack control on the microscale reduced both the alkali silica reaction rate and the corrosion rate.

Effect of crack control on ASR: Crack control due to steel microfibers leads to a chemo-mechanical confinement of the ASR gel. The resistance in crack propagation and crack opening displacement not only imposes compressive stresses on the expanding ASR gel but also prevents the ASR gel from leaving the reaction site. Preventing the ASR gel from leaving the reaction site increases the ion concentration of the ASR gel. The higher Si ion concentration of the ASR gel in the SMF reinforced specimen retards further dissolution of the reactive aggregate, thereby, reducing the ASR gel production and the ASR rate. The higher viscosity of the ASR gel in SMF reinforced specimens confirms the lack of escape of the reaction products away from the reaction site.

Effect of crack control on corrosion: The fibers may act in much the same way they did in the presence of ASR. In the case of conventional plain concrete, the formation of iron-oxides induces expansive stresses which cause microcracking. Once a crack has formed, the magnitude of expansive stress required to propagate the crack is reduced (see Fig. 3a) and the rate of egress of corrosion products is increased due to the crack opening. Microfibers close to the steel surface provide a source of passive confinement. Cracks can only propagate under increases in the magnitude of expansive stress (see Fig. 3b). In this way, expansive corrosion products that form near the surface of the steel bar remain there and collect. It is postulated that under this confined condition, the solid products formed from the corrosion process will fill surrounding voids and any cracks that may have initiated, locally densifying the cement matrix and cutting off further ingress of deleterious compounds.

REFERENCES

- ASTM C 1260-94. 1999. Standard test method for potential alkali reactivity of aggregates (mortar-bar method) in Annual book of ASTM Standards v. 04.02.
- CERF 2004, Civil Engineering Research Foundation (CERF) website; <http://www.cerf.org/conmat/hotprosp/frp2.htm>
- Banthia, N. & Soleimani, M. 2005. Flexural response of hybrid fiber-reinforced cementitious composites. *ACI Materials Journal* 102: 382-389.
- Blunt, J. & Ostertag, C.P. 2007. Performance based materials approach to bridge approach slabs. *ACI Materials Journal*, in press
- Gamry Echem Analyst. 2003. CD-ROM. Warminster, Pennsylvania: Gamry Instruments, Inc. Version 1.30.
- Grupp, J.A., Blunt, J., Ostertag, C.P. & Devine, T.M. 2007. Effect of steel microfibers on corrosion of steel reinforcing bars. *Cem. Concr. Research*, in press
- Helmuth, R. & Stark, D. 1989. Alkali-silica reactivity mechanisms. *Mat. Sci. of Concrete III*, ed. by J. Skalny & S. Mindess, , Am. C. Soc., Westernville, OH., 131-208.
- Ostertag, C.P. & Yi, CK. 2007. Crack/fiber interaction and crack growth resistance behavior in microfiber reinforced mortar specimens. *Materials and Structures*, in press.
- Qian, C. & Stroeven, P. 2000. Development of hybrid polypropylene steel fiber reinforced concrete. *Cem. Concr. Res.* 30: 63-69.
- Rostam, S. 2001. Design for durability: the great belt link. *Concrete Technology: New Trends, Industrial Applications*. Ed. by A. Auguado, R. Gettu, and S.P. Shah. RILEM.
- Vail, J.G. 1952. Soluble silicates, their properties and uses, Vol1: Chemistry; ACS Monograph No. 116, Reinhold Pub. Corporation
- Yi, CK. & Ostertag, C.P. 2002. Strengthening and toughening mechanisms in microfiber reinforced cementitious composites. *J. Mat. Sci.* 36: 1513-1522.
- Yi, CK. & Ostertag, C.P. 2005. Mechanical approach in mitigating alkali silica reaction. *Cem. Concr. Res.* 35: 67-76.